

# Study of muons from ultrahigh energy cosmic ray air showers measured with the Telescope Array experiment

R. Takeishi<sup>1,\*</sup> on behalf of the Telescope Array Collaboration

<sup>1</sup>Department of Physics, Sungkyunkwan University, Jang-an-gu, Suwon, Korea

**Abstract.** One of the uncertainties in ultrahigh energy cosmic ray (UHECR) observation derives from the hadronic interaction model used for air shower Monte-Carlo (MC) simulations. One may test the hadronic interaction models by comparing the measured number of muons observed at the ground from UHECR induced air showers with the MC prediction. The Telescope Array (TA) is the largest experiment in the northern hemisphere observing UHECR in Utah, USA. It aims to reveal the origin of UHECRs by studying the energy spectrum, mass composition and anisotropy of cosmic rays by utilizing an array of surface detectors (SDs) and fluorescence detectors. We studied muon densities in the UHE extensive air showers by analyzing the signal of TA SD stations for highly inclined showers. On condition that the muons contribute about 65% of the total signal, the number of particles from air showers is typically  $1.88 \pm 0.08$  (stat.)  $\pm 0.42$  (syst.) times larger than the MC prediction with the QGSJET II-03 model for proton-induced showers. The same feature was also obtained for other hadronic interaction models, such as QGSJET II-04.

## 1 Introduction

The Telescope Array (TA) experiment [1] observes ultrahigh energy cosmic rays (UHECRs) in Utah, USA. The scientific goals of the TA include determination of the energy spectrum, mass composition and anisotropy of UHECRs. It aims to reveal the origin of UHECRs by studying them.

The information of cosmic rays is estimated from observed signals of air showers, which are particle cascades generated in the atmosphere, and the air shower Monte Carlo (MC) simulation. Inferences of UHECR mass composition from air shower measurements are model-dependent [2, 3] since the air shower MC for cosmic rays at energies above  $10^{18}$  eV uses the extrapolated values of the hadronic interaction parameters. The difference in interaction parameters between hadronic interaction models is due to the uncertainty of modeling pion or kaon generation at the early stage of the air shower development.

The Pierre Auger Observatory, which is located in Mendoza, Argentina, reported a model-dependent deficit of muons in simulations of 30–80% relative to the data at an energy of  $10^{19}$  eV [4]. The Auger group also reported that the observed hadronic signal in UHECR air showers is  $1.61 \pm 0.21$  ( $1.33 \pm 0.16$ ) times larger than the post-LHC MC prediction values for QGSJET II-04 [5] (EPOS-LHC [6]), including statistical and systematic errors [7]. These reports suggest that present hadronic interaction models do not fully reproduce air showers.

The number of muons from a UHECR on the ground depends on the mass composition of primary cosmic rays. The MC prediction depends also on hadronic interaction

models since it has information about the shower development at an early stage. It is useful to compare the measured number of muons with the MC prediction for improving hadronic interaction models. In this paper, we present the study of differences in the number of muons between experimental data and the MC.

## 2 Detector

The TA experiment consists of the surface detectors (SDs) and the fluorescence detectors (FDs). The TA SD is designed to measure air shower particles on the ground. The TA SD array consists of 507 scintillation counters, placed on a square grid with 1.2 km spacing, covering 700 km<sup>2</sup> [8]. Each TA SD is composed of two layers of plastic scintillator with two photomultiplier tubes (PMTs), one for each layer. It has an area of 3 m<sup>2</sup> and each layer has 1.2 cm thickness. Air shower particles generate photons in scintillators and they are detected with PMTs through wavelength shifting fibers. The SD array trigger is created when at least three adjacent counters detect energy deposits equivalent or greater than the one corresponding to three minimum ionizing particles (MIPs) within 8 microseconds. The readout system then records SD signals equivalent to  $\geq 0.3$  MIP detected within  $\pm 32$  microseconds of the trigger time. The trigger efficiency is greater than 97% for primary particles with energies above  $10^{19}$  eV [8]. The TA SD is sensitive to the electromagnetic (EM) component (electrons and gammas) that are the predominant part of secondary particles from the air showers. The TA FD is designed to measure fluorescence light induced by the air shower. The three TA FD stations are located around the SD array and view the sky above the array [9].

\*e-mail: [takeishi@skku.edu](mailto:takeishi@skku.edu)

The TA SD event reconstruction consists of the following steps [10]: First, air shower SD signals are selected by determining a cluster which is contiguous in space and time. This process reduces the random atmospheric muon background, which occurs uniformly in space and time at a rate of 0.05 per station within one event period ( $\pm 32$  microseconds). Second, a time fit of shower arrivals at the SDs is performed to determine the geometry of air showers. Third, the lateral distribution of charged particle densities at the SDs is fit using the AGASA lateral distribution function [11, 12]. The density of shower particles at a lateral distance of 800 m from the air shower axis is called  $S_{800}$ . The energy of the cosmic ray is estimated by using a look-up table in  $S_{800}$  and the shower zenith angle. The table is obtained by a large statistics MC simulation using CORSIKA [13] and the QGSJET II-03 hadronic model [14]. Finally, the reconstructed energy is scaled to the energy measured by the TA FD. The FD utilizes calorimetric detection of an air shower energy deposition in the atmosphere [9, 15, 16] with less hadronic interaction dependence than the SD. The energy and angular resolutions for a primary energy within  $10^{18.5}$  eV  $< E < 10^{19.0}$  eV are 29% and 2.1°, respectively [17]. Those for energies above  $10^{19}$  eV are 19% and 1.4°, respectively.

To perform the MC, we use CORSIKA v6.960, and QGSJET II-03 as a reference model for high energy hadronic interactions. We also use FLUKA2008.3c [18, 19] to model low energy hadronic interactions and EGS4 [20] to model electromagnetic interactions. The thinning [21] and “de-thinning” [22] techniques are used to reduce the computation time. The detector simulation is done by using the Geant4 [23] toolkit. The simulated cosmic ray energies range from  $10^{16.55}$  to  $10^{20.55}$  eV, and the zenith angle is isotropically distributed from 0° to 60°. The azimuth angle and core position are randomly distributed within the SD array. The reconstruction procedure for the MC is the same as for experimental data.

### 3 Analysis method

We use the TA SD dataset over seven years, recorded from 11 May 2008 to 11 May 2015, and the events reconstructed by the same method as the TA spectrum analysis [24] with an energy range  $10^{18.8}$  eV  $< E < 10^{19.2}$  eV. In this energy range, the mass composition of the primary cosmic rays estimated by the FD measurement is consistent with a light component within statistical and systematic errors [2, 3, 15, 25], thus we use the MC for proton primaries. We used the energy scale corrected by the FD (reconstructed energy scale) for the experimental data and the scale not corrected by the FD (thrown energy scale) for the MC. The correction factor is 27%, which corresponds to a difference of about 20-30% in signal sizes of SDs at a lateral distance of 800 m. We compare experimental data with the MC using the hadronic interaction models QGSJET II-03, QGSJET II-04, Epos 1.99 [26] and Sibyll 2.1 [27].

The air shower secondary particles generated in the atmosphere are attenuated by the interaction with atmospheric particles and they decay before they reach the

ground. The EM components experience greater attenuation than muons over the same path length. Hence the ratio of the energy deposit of air shower muons to that of all particles (air shower and background components) in SD signals is expected to be larger for SDs more distant from the shower axis above the ground. Hereafter this ratio is described as the *muon purity*. We classify the detector hits in the air shower events of the dataset using  $\theta$  (the zenith angle),  $\phi$  (the azimuth angle relative to the shower arrival direction projected onto the ground), and  $R$  (the distance from a shower axis). The geometry definition is described in Figure 1. The muon purity in SD signals is expected to be higher for larger  $\theta$ ,  $|\phi|$  or  $R$  values.

The integrated FADC is calculated for each SD related to the air shower event. The FADC count, converted to Vertical Equivalent Muon (VEM) units, is entered in the histogram of the corresponding  $(\theta, \phi, R)$  bin. An SD which has no signal is assigned to the 0 VEM bin of the histogram. Figure 2 shows the lateral distributions of SD signals and the muon purity. The muon purity is mainly 60-70% on the high muon purity condition ( $30^\circ < \theta < 45^\circ$ ,  $150^\circ < |\phi| < 180^\circ$ ,  $2000 \text{ m} < R < 4000 \text{ m}$ ). We use these conditions to select high muon purity events for the comparison of the data with the MC.

The statistical error of the average signal cannot be simply calculated for  $R \gtrsim 1500$  m. The difficulty originates because the fraction of SDs with no hit signals is too large to determine lower and upper errors from the shape of the signal size distribution. We assume the Poisson distribution  $f(x) = N^x e^{-N} / x!$ ;  $N$  is the average value of the distribution and  $x$  is the variable for the signal size distribution. We calculated the average signal by the following equation:  $n_0/n_{\text{all}} = f(0) = e^{-N}$ . Here  $n_0$  and  $n_{\text{all}}$  are the number of 0 VEM SDs and the total number of SDs related to an air shower event. The probability that zero values appear  $n_0$  times in  $n_{\text{all}}$  samples follows the binomial distribution, hence the standard deviation of  $n_0$  is calculated as  $\sqrt{n_{\text{all}} p(1-p)}$ , where  $p$  is  $n_0/n_{\text{all}}$ .

The systematic error is dominated by the uncertainty of the TA FD energy measurement, which is 21% [16]. The total systematic error of this work is  $\pm(22-24\%)$ .

### 4 Results

Figure 3 shows the lateral distributions of the signal and the ratio of the data to the MC with the hadronic interaction models QGSJET II-03, QGSJET II-04, Epos 1.99 and Sibyll 2.1. The average ratios of the data to the MC with QGSJET II-03 are calculated to be  $1.72 \pm 0.10(\text{stat.}) \pm 0.37(\text{syst.})$  at  $1910 \text{ m} < R < 2160 \text{ m}$  and  $3.14 \pm 0.36(\text{stat.}) \pm 0.69(\text{syst.})$  at  $2760 \text{ m} < R < 3120 \text{ m}$ . The ratios of the data to the MC with QGSJET II-04 are  $1.67 \pm 0.10(\text{stat.}) \pm 0.36(\text{syst.})$  at  $1910 \text{ m} < R < 2160 \text{ m}$  and  $2.75 \pm 0.32(\text{stat.}) \pm 0.60(\text{syst.})$  at  $2760 \text{ m} < R < 3120 \text{ m}$ . The observed lateral distribution (circles) decreases less with radial distance than that of all hadronic interaction models (other points). The data becomes closer to the MC at  $R \gtrsim 4000$  m, since the atmospheric muon background dominates the SD signals at the distance.

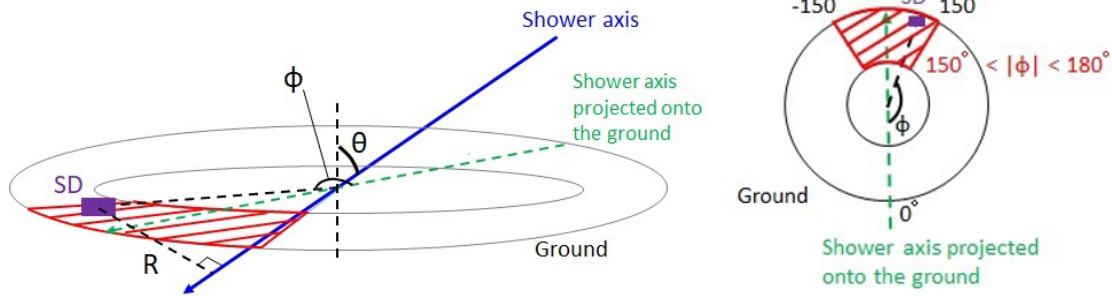


**Figure 1.** (left) Geometry definition of the muon analysis. There are six bins for  $\phi$  and 18 bins for  $R$  from 500 to 4500 m. The red shaded region in the figure shows the bin for  $150^\circ < |\phi| < 180^\circ$ , which is expected to be the bin with less EM background. (right) Top view for the  $\phi$  definition.

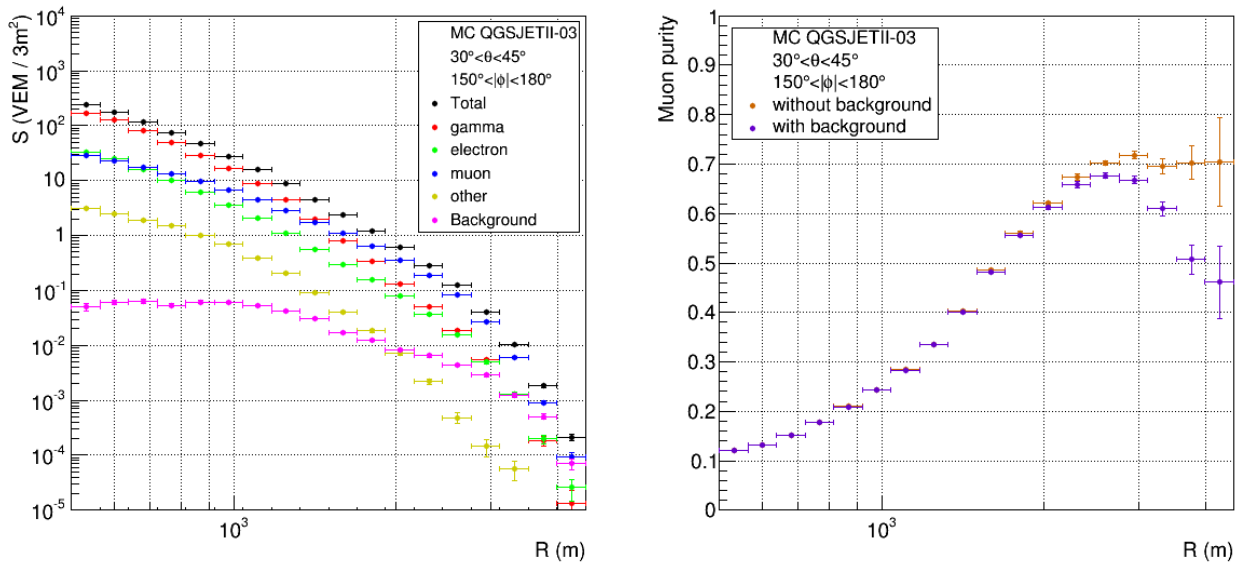


**Figure 2.** Lateral distributions of the air shower MC with QGSJET II-03 for  $30^\circ < \theta < 45^\circ$ ,  $150^\circ < |\phi| < 180^\circ$ ,  $500 \text{ m} < R < 4500 \text{ m}$  [28]. (left) The signal size for each particle type. The vertical error bar shows the standard deviation. (right) The muon purity. The violet and orange dots show results calculated with and without the atmospheric muon background, respectively.

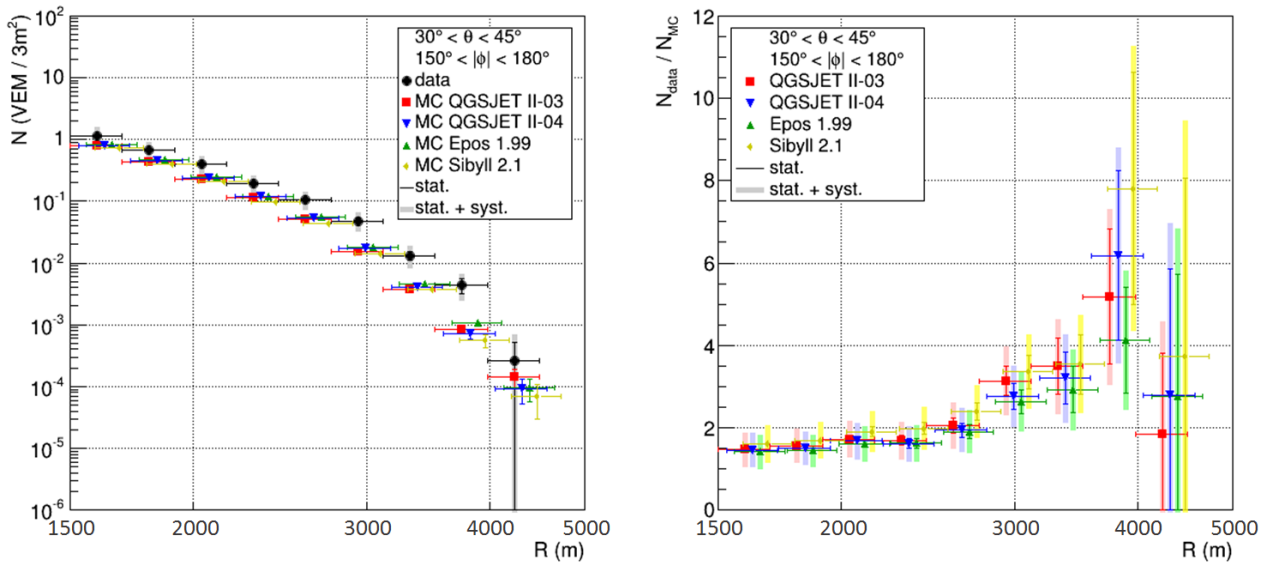
We calculated lateral distributions for iron showers using the MC with QGSJET II-03. Figure 4 shows lateral distributions of the ratio of the data to the MCs for proton and iron showers. The average signal of the data is larger than the MC for iron showers at  $R \gtrsim 2500 \text{ m}$ . For the smaller distances, the difference between the data and the MC for iron showers is smaller than the systematic errors.

Figure 5 shows the correlation between the muon purity expected from the MC and the ratio of the signal size to that of the MC. We loosened the cut condition for the zenith angle of air showers from  $45^\circ$  to  $55^\circ$  to see the correlation precisely. On the high muon purity condition ( $30^\circ < \theta < 45^\circ$ ,  $150^\circ < |\phi| < 180^\circ$ ,  $2000 \text{ m} < R < 4000 \text{ m}$ ), represented by the magenta filled circle in Figure 5), the muon purity and the ratio of the data to the MC are  $65\%$  and  $1.88 \pm 0.08(\text{stat.}) \pm 0.42(\text{syst.})$ , respectively. In the case of the low muon purity condition ( $\theta < 30^\circ$ ,  $|\phi| < 30^\circ$ ,  $2000 \text{ m} < R < 4000 \text{ m}$ ), represented by

the black open circle in Figure 5), they are calculated to be  $28\%$  and  $1.30 \pm 0.06(\text{stat.}) \pm 0.29(\text{syst.})$ , respectively. This figure shows larger differences in signal sizes between the data and the MC for conditions of higher muon purity.

## 5 Conclusion

We presented the study of muons in UHECR-induced air showers detected by the TA SD. For that, an analysis of muons from UHECR air showers with the TA scintillator SDs was developed. The air shower events and the locations of SDs were binned in  $\theta$ ,  $\phi$  and  $R$  in order to determine events with a high muon purity. Air shower signals on the high muon purity condition ( $30^\circ < \theta < 45^\circ$ ,  $150^\circ < |\phi| < 180^\circ$ ,  $2000 \text{ m} < R < 4000 \text{ m}$ ) for  $10^{18.8} \text{ eV} < E < 10^{19.2} \text{ eV}$  indicated an excess in the data compared to the MC. On that condition, the muon purity expected from the MC is  $\sim 65\%$  and the ratios of the signal



**Figure 3.** Lateral distributions of air showers for  $30^\circ < \theta < 45^\circ$ ,  $150^\circ < |\phi| < 180^\circ$ ,  $500 \text{ m} < R < 4500 \text{ m}$  [28]. (left) The signal size of data with the MCs using various hadronic models. To make error bars easy to see, the plots for the latter three models are shifted to the right. (right) The average ratio of the data to the MC.

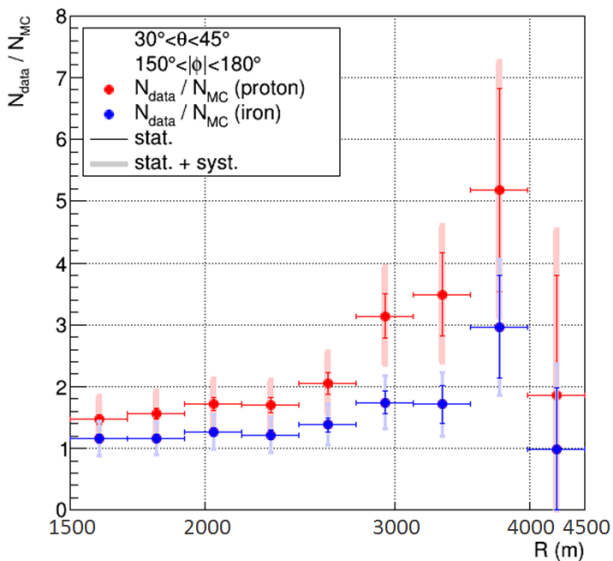


**Figure 4.** Ratios of the signal size of the data to the MCs for proton and iron showers [28]. The vertical thin error bars and shaded thick error bars represent statistical errors and quadratic sums of statistical and systematic errors, respectively.

size of the data to that of the MC with QGSJET II-03 are  $1.72 \pm 0.10(\text{stat.}) \pm 0.37(\text{syst.})$  at  $1910 \text{ m} < R < 2160 \text{ m}$  and  $3.14 \pm 0.36(\text{stat.}) \pm 0.69(\text{syst.})$  at  $2760 \text{ m} < R < 3120 \text{ m}$ . This excess feature also appeared when we used different MC models including QGSJET II-04.

The primary effect found in this work, that the muon signal is larger in the data than predicted by the MC, is

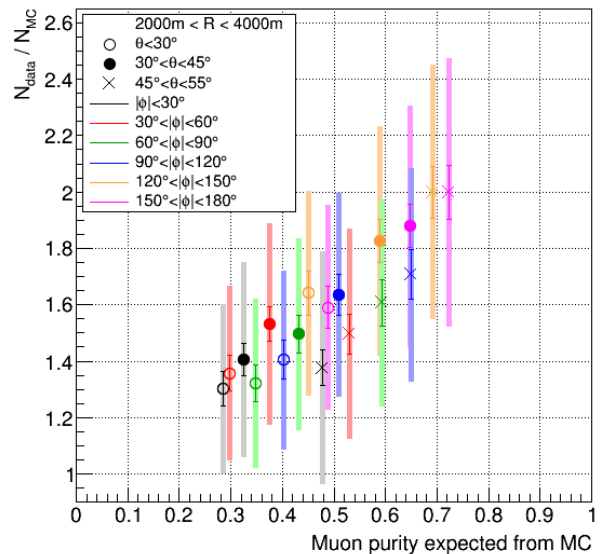


**Figure 5.** The correlation between the muon purity and the ratio of the signal size of the data to the MC with QGSJET II-03 for  $2000 \text{ m} < R < 4000 \text{ m}$  [28]. The vertical thin error bars and shaded thick error bars represent statistical errors and quadratic sums of statistical and systematic errors, respectively.

qualitatively consistent with the excesses of muons reported by the Auger experiment. In addition to that, we found larger differences between the data and the MC at larger lateral distances.

## Acknowledgments

The Telescope Array experiment is supported by the Japan Society for the Promotion of Science (JSPS) through Grants-in-Aid for Priority Area 431, for Specially Promoted Research JP21000002, for Scientific Research (S) JP19104006, for Specially Promoted Research JP15H05693, for Scientific Research (S) JP15H05741 and for Young Scientists (A) JPH26707011; by the joint research program of the Institute for Cosmic Ray Research (ICRR), The University of Tokyo; by the U.S. National Science Foundation awards PHY-0601915, PHY-1404495, PHY-1404502, and PHY-1607727; by the National Research Foundation of Korea (2017K1A4A3015188; 2016R1A2B4014967; 2017R1A2A1A05071429, 2016R1A5A1013277); by the Russian Academy of Sciences, RFBR grant 16-02-00962a (INR), IISN project No. 4.4502.13, and Belgian Science Policy under IUAP VII/37 (ULB). The foundations of Dr. Ezekiel R. and Edna Wattis Dumke, Willard L. Eccles, and George S. and Dolores Doré Eccles all helped with generous donations. The State of Utah supported the project through its Economic Development Board, and the University of Utah through the Office of the Vice President for Research. The experimental site became available through the cooperation of the Utah School and Institutional Trust Lands Administration (SITLA), U.S. Bureau of Land Management (BLM), and the U.S. Air Force. We appreciate the assistance of the State of Utah and Fillmore offices of the BLM in crafting the Plan of Development for the site. Patrick Shea assisted the collaboration with valuable advice on a variety of topics. The people and the officials of Millard County, Utah have been a source of steadfast and warm support for our work which we greatly appreciate. We are indebted to the Millard County Road Department for their efforts to maintain and clear the roads which get us to our sites. We gratefully acknowledge the contribution from the technical staffs of our home institutions. An allocation of computer time from the Center for High Performance Computing at the University of Utah is gratefully acknowledged.

## References

- [1] M. Fukushima, *Prog. Theor. Phys. Suppl.* **151**, 206 (2003).
- [2] T. Stroman *et al.*, *Proc. 34th ICRC*, 361 (2015).
- [3] T. Fujii *et al.*, *Proc. 34th ICRC*, 320 (2015).
- [4] A. Aab *et al.* (Pierre Auger Collaboration), *Phys. Rev. D* **91**, 032003 (2015); Erratum, *Phys. Rev. D* **91**, 059901 (2015).
- [5] S. Ostapchenko, *Phys. Rev. D* **83**, 014018 (2011).
- [6] K. Werner, F. M. Liu, and T. Pierog, *Phys. Rev. C* **74**, 044902 (2006).
- [7] A. Aab *et al.* (Pierre Auger Collaboration), *Phys. Rev. Lett.* **117**, 192001 (2016).
- [8] T. Abu-Zayyad *et al.*, *Nucl. Instrum. Methods. A* **689**, 87 (2012).
- [9] R.U. Abbasi *et al.*, *Astropart. Phys.* **80**, 131 (2016).
- [10] D. Ivanov, Ph.D. thesis, Rutgers-The State University of New Jersey, Department of Physics and Astronomy, Piscataway, New Jersey, USA (2012).
- [11] M. Takeda *et al.*, *Phys. Rev. Lett.* **81**, 1163 (1998).
- [12] M. Takeda *et al.*, *Astropart. Phys.* **19**, 447 (2003).
- [13] D. Heck *et al.*, *Forschungszentrum Karlsruhe Report FZKA*, 6019 (1998).
- [14] S. Ostapchenko, *Nucl. Phys. B, Proc. Suppl.* **151**, 147 (2006).
- [15] D. Ikeda *et al.*, *Proc. 34th ICRC* 362 (2015).
- [16] T. Abu-Zayyad *et al.*, *Astropart. Phys.* **61**, 93 (2015).
- [17] R. U. Abbasi *et al.*, *Astropart. Phys.* **86**, 21 (2017).
- [18] A. Ferrari *et al.*, *Tech. Rep. 2005-010*, CERN (2005).
- [19] G. Battistoni *et al.*, *AIP Conf. Proc.* **896**, 31 (2007).
- [20] W. R. Nerson *et al.*, *Tech. Rep. 0265* SLAC (1985).
- [21] M. Kobal *et al.*, *Astropart. Phys.* **15**, 259 (2001).
- [22] B. T. Stokes *et al.*, *Astropart. Phys.* **35**, 759 (2012).
- [23] J. Allison *et al.*, *IEEE Trans. Nucl. Sci.* **53**, 270 (2006).
- [24] T. Abu-Zayyad *et al.*, *ApJ* **768**, L1 (2013).
- [25] R.U. Abbasi *et al.*, *Astropart. Phys.* **64**, 49 (2015).
- [26] T. Pierog and K. Werner, *Nucl. Phys. Proc. Suppl.* **196**, 102 (2009).
- [27] E. J. Ahn *et al.*, *Phys. Rev. D* **80**, 094003 (2009).
- [28] R. U. Abbasi *et al.* (Telescope Array Collaboration), *Phys. Rev. D* **98**, 022002 (2018).